OXFORD

Cerebral Cortex, July 2020;30: 4110–4120

doi: 10.1093/cercor/bhaa034
Advance Access Publication Date: 12 March 2020
Original Article

ORIGINAL ARTICLE

APOE-ε4 Shapes the Cerebral Organization in Cognitively Intact Individuals as Reflected by Structural Gray Matter Networks

Raffaele Cacciaglia[1,2,3], José Luis Molinuevo[1,2,3,4], Carles Falcón[1,2,5], Eider M. Arenaza-Urquijo[1,2,3], Gonzalo Sánchez-Benavides[1,2,3], Anna Brugulat-Serrat[1,2,3,6], Kaj Blennow[7,8], Henrik Zetterberg[7,8,9,10] and Juan Domingo Gispert[1,2,4,5] for the ALFA study

[1]Barcelonaβeta Brain Research Center (BBRC), Pasqual Maragall Foundation, 08005 Barcelona, Spain, [2]Hospital del Mar Medical Research Institute (IMIM), 08005 Barcelona, Spain, [3]Centro de Investigación Biomédica en Red de Fragilidad y Envejecimiento Saludable (CIBERFES), 28089 Madrid, Spain, [4]Universitat Pompeu Fabra, 08002 Barcelona, Spain, [5]Centro de Investigación Biomédica en Red de Bioingeniería, Biomateriales y Nanomedicina (CIBERBBN), 28089 Madrid, Spain, [6]Global Brain Health Institute, University of California San Francisco, San Francisco, CA 94115, USA, [7]Department of Psychiatry and Neurochemistry, Institute of Neuroscience and Physiology, The Sahlgrenska Academy at the University of Gothenburg, 41390 Mölndal, Sweden, [8]Clinical Neurochemistry Laboratory, Sahlgrenska University Hospital, 41390 Mölndal, Sweden, [9]UK Dementia Research Institute at UCL, WC1E 6BT London, UK and [10]Department of Neurodegenerative Disease, UCL Institute of Neurology, WC1N 3BG London, UK

Address correspondence to Raffaele Cacciaglia and Juan Domingo Gispert López, Barcelonaβeta Brain Research Center, Pasqual Maragall Foundation, Wellington 30, 08005 Barcelona, Spain. Email: rcacciaglia@barcelonaneta.org; jdgispert@barcelonaneta.org.

The complete list of collaborators of the ALFA study can be found in the Notes section.

Abstract

Gray matter networks (GMn) provide essential information on the intrinsic organization of the brain and appear to be disrupted in Alzheimer's disease (AD). Apolipoprotein E (*APOE*)-ε4 represents the major genetic risk factor for AD, yet the association between *APOE*-ε4 and GMn has remained unexplored. Here, we determine the impact of *APOE*-ε4 on GMn in a large sample of cognitively unimpaired individuals, which was enriched for the genetic risk of AD. We used independent component analysis to retrieve sources of structural covariance and analyzed *APOE* group differences within and between networks. Analyses were repeated in a subsample of amyloid-negative subjects. Compared with noncarriers and heterozygotes, *APOE*-ε4 homozygotes showed increased covariance in one network including primarily right-lateralized, parietal, inferior frontal, as well as inferior and middle temporal regions, which mirrored the formerly described AD-signature. This result was confirmed in a subsample of amyloid-negative individuals. *APOE*-ε4 carriers showed reduced covariance between two networks encompassing frontal and temporal regions, which constitute preferential target of amyloid deposition. Our data indicate that, in asymptomatic individuals, *APOE*-ε4 shapes the cerebral organization in a way that recapitulates focal morphometric alterations observed in AD patients, even in absence of amyloid pathology. This

suggests that structural vulnerability in neuronal networks associated with APOE-ε4 may be an early event in AD pathogenesis, possibly upstream of amyloid deposition.

Key words: Alzheimer's disease, *APOE*, gray matter networks, independent component analysis, processing speed

Introduction

Alzheimer's disease (AD) is characterized by a distinctive pattern of brain atrophy along with progressive decline in multiple cognitive domains (Braskie and Thompson, 2013). Core pathological hallmarks of AD are cerebral extracellular deposition of beta-amyloid (Aβ) fibrils and intraneuronal aggregation of hyperphosphorylated tau protein (Frisoni et al., 2017). Abnormally low cerebral glucose metabolism, as assessed with 2-[^{18}F]fluoro-2-deoxy-D-glucose (FDG) positron emission tomography (PET), is also present across several regions including temporo-parietal and posterior cingulate cortices (Alexander et al., 2002; Mosconi, 2013). Yet, preclinical signatures of the disease in asymptomatic individuals are already evident at least two decades prior to cognitive impairment, opening a temporal window, which is critical to delay the onset of dementia (Sperling et al., 2011). The preclinical course of AD is influenced by multiple genetic markers (Escott-Price et al., 2015; Tan et al., 2017). Among those, apolipoprotein E (*APOE*)-ε4 represents the greatest genetic risk factor for AD, by lowering the age of onset in a dose-dependent manner (Corder et al., 1993; Farrer et al., 1997). The ε4 allele codes the E4 isoform of the *APOE* protein, which is associated to a deficient neuronal cholesterol delivery, as well as poor clearance of extracellular Aβ, therefore facilitating the formation of fibrillary plaques (Liu et al., 2013). In cognitively unimpaired individuals, *APOE*-ε4 has been related to faster rates of cerebral Aβ accumulation (Reiman et al., 2009; Jansen et al., 2015), as well as lower brain glucose metabolism (Reiman et al., 2005). These effects appear to be dose-dependent, that is, proportional to the number of *APOE*-ε4 alleles (see Fouquet et al., 2014 for a review). With respect to brain structure, some previous studies have reported significantly different gray matter volumes in healthy ε4-carriers compared with noncarriers (NC) in regions typically associated to AD degeneration, such as the hippocampus, frontal, and temporal areas (Honea et al., 2009; Alexander et al., 2012; Ten Kate et al., 2016). We have recently reported dose-dependent effects of the risk allele on posterior hippocampal volume and on other areas in a sample of cognitively unimpaired individuals that was genetically enriched for the presence of *APOE*-ε4 homozygotes (Cacciaglia et al., 2018a). However, the adoption of a univariate statistical approach prevented us to investigate the role of *APOE*-ε4 on the structural organization of the brain.

The adoption of multivariate methods for the study of cerebral anatomy allows the detection of gray matter networks (GMn), which are expression of the coordinated volumetric variability across several brain areas. Unlike univariate voxel-based or region of interest analyses, this approach provides essential information on the intrinsic organization of cerebral morphology and it may thus capture subtle differences not yet observable with traditional approaches (Alexander-Bloch et al., 2013; Guo et al., 2014). GMn have been studied in relation to cognitive abilities in healthy people (Eckert et al., 2010; Yoon et al., 2017), as well as in psychiatric (Xu et al., 2009; Kasparek et al., 2010) and neurologic (Steenwijk et al., 2016) disorders. For example, AD patients show significantly reduced structural covariance within the regions of the default mode network (DMN) (Seeley et al., 2009; Spreng and Turner, 2013). Yet, most of the studies investigating GMn have relied on the selection of a seed region to identify common cerebral networks, such as the DMN, salience, or the executive control (Evans, 2013). While this approach has the advantage of studying brain systems that are known to regulate cognitive functions, it prevents from uncovering additional hidden sources of variance, which may be subject to preclinical alterations in asymptomatic individuals.

Therefore, the goal of the present study was to investigate GMn as a function of the *APOE* genotype using a data-driven, spatially unbiased approach, to provide further insights on the structural vulnerability associated to the genetic risk for AD. We assessed both within- and between-networks structural covariance, capitalizing on a large sample ($n = 533$) of cognitively unimpaired individuals, which was enriched for the genetic risk of AD by hosting an unprecedented number of *APOE*-ε4 homozygotes for a single-site imaging study ($n = 65$). This sample characteristic allowed us to test different models of genetic penetrance enabling to pinpoint distinctive cerebral features as a function of the allelic load. In addition, to better characterize GMn, we determined their association with age and cognitive performance in the entire sample. In order to rule out the influence of amyloid pathology in our findings, we repeated the analyses on a subsample of participants that was amyloid-negative.

Materials and Methods

Study Participants

Participants were enrolled to the ALFA (ALzheimer and FAmilies) study (Clinicaltrials.gov Identifier: NCT01835717), a research platform aiming at the identification of pathophysiological alterations in preclinical AD. The ALFA cohort entangles 2743 cognitively unimpaired individuals, with a Clinical Dementia Rate score of 0, most of them being first-order descendants of AD patients (Molinuevo et al., 2016). Subjects with a psychiatric diagnosis were excluded from the study. Additional exclusion criteria were described in detail previously (Molinuevo et al., 2016). After *APOE* genotyping, which is described in detail in the Supplementary Material, all participants homozygous for the ε4 allele as well as carriers of the ε2 allele were invited to undergo magnetic resonance imaging (MRI) scanning along with ε4-heterozygotes (ε4HET) and NC matched for age and sex. This recruitment strategy resulted in 576 study participants, out of which 43 had to be discarded due to MRI incidental findings or poor image quality, leading to a final sample of 533 individuals. For the statistical analyses, participants were pooled according to the cumulative presence of the ε4 allele, that is, NC, ε4HET and ε4-homozygotes (ε4HMZ). The study was approved by the local ethics committee and conducted according to the principles expressed in the Declaration of Helsinki, with all subjects providing written informed consent.

Image Data Acquisition and Preprocessing

MRI was conducted with the same MR equipment and in a single site for each study participant (3 T General Electric scanner, GE

Discovery MR750 W). Structural 3D high-resolution T1-weighted images were collected using a fast spoiled gradient-echo sequence with the following parameters: voxel size = 1 mm^3 isotropic, repetition time (TR) = 6.16 ms, echo time (TE) = 2.33 ms, inversion time (TI) = 450 ms, matrix size = 256 × 256 × 174, and flip angle = 12°. The new segment function implemented in Statistical Parametrical Mapping software (SPM 12, Wellcome Department of Imaging Neuroscience, London, UK) was used to segment gray matter in native space and locate all images into a common reference space for subsequent normalization, using a 12-affine parameter transformation. Segmented GM images were used to generate a reference template of the sample, which was warped into a standard Montreal Neurological Institute (MNI) space using the high-dimensional DARTEL toolbox (Ashburner, 2007). The generated flow fields and normalization parameters were then implemented to normalize the native GM images to the MNI space. In order to preserve the native local amount of GM volume, we applied a modulation step, where each voxel signal's intensity was multiplied by the Jacobian determinant derived from the normalization procedure (Good et al., 2001). Quality control of normalization was assured by checking the sample homogeneity with the computational anatomy toolbox (CAT12) (http://dbm.neuro.uni-jena.de/cat/) using nonsmoothed data, which did not return errors in the registration procedure in any subject. Finally, images were spatially smoothed with a 6-mm full-width at half maximum Gaussian kernel. Total intracranial volume (TIV) was computed by summing the segmented GM, white matter (WM), and cerebrospinal fluid (CSF) volumes for each individual.

Assessment of the Gray Matter Networks

After preprocessing, GMn were assessed from normalized and smoothed images using source-based morphometry (SBM) (Xu et al., 2009), implemented in the GIFT software (http://mialab.mrn.org/software/gift/index.html). SBM uses independent component analysis (ICA) to decompose signal intensity across the images into sources of common variance. This procedure uses variance in the data to detect brain regions that covary in terms of gray matter volume, and therefore represent a structural network. We used the Infomax neural network algorithm, which iteratively minimizes the mutual information of the network outputs to identify naturally grouping and maximally independent sources (Bell and Sejnowski, 1995). The number of independent components was estimated data-driven on the basis of the computation of the correspondent latent principal components. This was achieved using the minimum description length criteria (Li et al., 2007). To increase component reliability and consistency, we used the ICASSO algorithm (Himberg et al., 2004) and repeated ICA 250 times with bootstrapping and random initialization. Each individual gray matter image was converted into a 1D vector and arrayed into a matrix of number of subject by each voxel's intensity. This group image matrix was then decomposed into a mixing matrix, representing the weights of each component for each subject, and a source matrix, representing the relationship between each component and brain voxels. The mixing matrix contained the loadings for each component, which were submitted to group statistical analyses. After components estimation, we removed those with poor clustering as revealed by a quality index $I_q < 0.8$ indicating the difference between intracluster and extracluster similarity (Himberg et al., 2004). Remaining components were visually inspected to select those of biological relevance. In so doing, we removed components containing sharp edges near to the brain parenchyma, or primarily appearing in nongray matter areas (i.e., WM or ventricles), as previously recommended (Xu et al., 2009).

Neuropsychological Evaluation

We evaluated episodic memory (EM) and processing speed (PS), two cognitive domains that have been included in the preclinical Alzheimer cognitive composite (Donohue et al., 2014) and for which we have already delineated the underlying cerebral morphology in a subsample of the present study (Cacciaglia et al., 2018b, 2019). EM was assessed with the Spanish adapted version of the memory binding test (Gramunt et al., 2016), an instrument that was developed for the detection of subtle impairments in the healthy population (Buschke, 2014). A description of the administration procedure is available at the online Supplementary Material. PS was assessed with the coding subtest of the Wechsler Adult Intelligence Scale-Fourth Edition (Wechsler, 2012), where participants are given keys that match numeric digit spanning from 1 to 9 with a symbol. The task is to write down the correct symbol aside a list of numbers as quickly as possible.

CSF Sampling and Analysis

CSF was sampled on average 4.11 years after MRI data acquisition. Fresh CSF samples were collected in 15 mL polypropylene tubes (Sarstedt catalog #62.554), the supernatant aliquoted into 0.5 mL polypropylene tubes (Sarstedt catalog #72.730.005), and frozen within 2 h after lumbar puncture. Aliquots were placed into long-term storage boxes and stored at −80 °C until shipment on dry ice for analysis. CSF samples were measured using the Elecsys β-amyloid (1–42) (Bittner et al., 2016), and the Elecsys phosphotau (181P) and Elecsys total-tau immunoassays for CSF on a cobas e 601 analyzer (software version 05.02) at the Clinical Neurochemistry Laboratory, University of Gothenburg, Sweden. Individuals with CSF Ab42 values below 1098 pg/mL were categorized as negative (Schindler et al., 2018).

Statistical Analyses

The impact of *APOE*-ε4 on GMn was determined separately for within- and between-networks structural covariance. In the former case, we conducted an analysis of covariance (ANCOVA) with each component's factor loadings modeled as dependent variable, while including age, sex, and TIV as covariates. For the between-networks analysis, we repeated the same ANCOVA and additionally modeled, for any structural component as dependent variable, the interaction between *APOE*-ε4 and any other component. This interaction term captures the modulatory effect of *APOE*-ε4 on the structural coupling between any two components. In all models, *APOE*-ε4 group membership was entered as independent fixed factor. To this respect, we tested three different genetic models of penetrance: additive, dominant, and recessive. Briefly, an additive model predicts an incremental response of the quantitative trait according to the allelic load, whereas a dominant model predicts a common response to one or two copy of the risk allele (i.e., ε4-carriers vs. NC). Finally, a recessive model predicts a common response to zero or one copy of the risk allele (i.e., NC and ε4HET vs. ε4HMZ) (Clarke et al., 2011). To assess the linear association between age and GMn, two-tailed Pearson's correlation was performed

Table 1 Sample characteristics

	Total sample ($n = 533$)	NC ($n = 261$)	ε4HET ($n = 207$)	ε4HMZ ($n = 65$)	P-value
Age (y)	57.58 (7.43)	57.93 (7.53)	58.22 (7.41)	54.14 (6.18)	<0.01
Sex (F/M)	320/213	166/95	113/94	41/24	0.13
Education (y)	13.64 (3.56)	13.69 (3.62)	13.66 (3.53)	13.38 (3.46)	0.82
TIV (cm^3)	1490.11 (146.07)	1484.96 (155.17)	1495.41 (137.73)	1493.91 (135.20)	0.72
TPR	24.18 (4.46)	23.91 (4.81)	24.23 (4.20)	25.14 (3.69)	0.21[a]
TFR	16.54 (5.17)	16.45 (5.22)	16.29 (5.08)	17.66 (5.15)	0.60[a]
TDPR	23.90 (4.60)	23.65 (4.87)	23.94 (4.40)	24.82 (3.98)	0.27[a]
TDFR	16.89 (5.18)	16.58 (5.35)	16.90 (4.78)	18.11 (5.62)	0.29[a]
Coding	65.50 (15.20)	65.67 (15.83)	64.26 (14.85)	68.78 (13.28)	0.63[a]

Note: NC: noncarriers; ε4HET: ε4-heterozygotes; ε4HET: ε4-homozygotes; TIV: total intracranial volume; M: mean; SD: standard deviation; TPR: total paired recall; TFR: total free recall; TDPR: total delayed paired recall; and TDFR: total delayed free recall. Except for the categorical variable sex, numbers represent mean and SD.
[a]Corrected for age, sex, and years of education.

between each structural component's factor loading and age. Lastly, to detect the association between GMn and cognitive performance, two-tailed partial correlation controlling for age and sex was performed between each IC factor loading and cognitive scores in both EM and PS. All the results were considered significant at $P < 0.05$, after correction for multiple testing using false discovery rate (FDR) (Benjamini and Hochberg, 1995). Analyses were repeated in the amyloid-negative subsample.

Results

Participants' Demographics and Cognitive Data

Table 1 summarizes demographic information stratified across *APOE*-ε4 subgroups along with cognitive scores. NC, ε4HET, and ε4HMZ did not significantly differ in years of education, proportion of males/females, or TIV. Similarly, there were no significant differences in any cognitive variable after adjusting for covariates. However, ε4HMZ were significantly younger than both NC and ε4HET. For this reason, age was included as covariate in all subsequent analyses. The range of the assessed demographic and cognitive variables is provided in the Supplementary Material (see Supplementary Table 1).

APOE-ε4 and Gray Matter Networks: Within Network Analysis

Our ICA retrieved 45 ICs, which were reduced to 16 biologically relevant GMn of interest, upon applying the criteria described above. Figure 1 shows surface rendering of four exemplary GMn projected onto a mesh template, along with a chord diagram exemplifying the correlations among all networks in the entire sample.

The genotypic recessive model yielded a significant main effect of *APOE*-ε4 on IC29, where ε4HMZ showed higher structural covariance compared with both NC and ε4HET ($F_{4,533} = 8.71$; $P = 0.003$; and $P_{FDR} = 0.044$) (Fig. 2). This network (IC29) consisted of prominently right-lateralized regions including parietal, inferior frontal, as well as inferior and middle temporal regions (Table 2). In addition, the left angular gyrus and precuneus, as well as the left middle and inferior temporal cortex were included (Table 2). All of these regions were previously included within a composite region of interest known as AD-signature, which undergoes focal atrophy early in the course of AD (Bakkour et al., 2009, 2013; Dickerson et al., 2009, 2011). Figure 2A shows the spatial overlay between IC29 and a reconstruction of the AD-signature, which was performed on the basis of the regions provided in Dickerson et al. (2009). The additive model retrieved a nominally significant difference in the same component (IC29), which however did not survive correction for multiple testing ($F_{4,533} = 4.35$; $P = 0.013$; and $P_{FDR} = 0.239$). No other ICs showed significantly different values among the three genotype groups.

APOE-ε4 and Gray Matter Networks: Between Network Analysis

Of the tested genotypic models, the dominant one yielded a significant effect of *APOE*-ε4 ($F_{1,533} = 8.23$; $P = 0.004$; and $P_{FDR} = 0.048$) in modulating the linear association between IC10 and IC15 (Fig. 3A). IC10 included both medial and lateral aspects of the superior frontal cortex bilaterally, with the inclusion of the middle cingulate gyrus, while IC15 entangled the frontal poles as well as the bilateral middle temporal gyrus (Fig. 3B). Additionally, a nominally significant effect was observed under the same genotypic model and in the same direction for IC02 and IC17 (Fig. 3), which however did not survive correction for multiple testing ($F_{1,533} = 6.84$; $P = 0.009$; and $P_{FDR} = 0.094$). Overall, these results indicate that, when compared with NC, both ε4HET and ε4HMZ displayed reduced structural covariance between these couples of networks.

Complementary Analysis in CSF $A\beta_{42}$ Negative Individuals

To determine to what extent the observed effects were specific to *APOE* genetic variance, we reanalyzed data from a subsample of individuals who were classified as negative to CSF $A\beta_{42}$ in a retrospective analysis. While this approach is blind to the actual $A\beta_{42}$ values when MRI data were acquired, it allows to identify those who did not have amyloid pathology at that time. Of the entire sample ($n = 533$), CSF was available for 121 individuals. Of those, 71 were $A\beta$-negative (see Supplementary Table 2 for a sample description). This analysis showed that, in the subsample with available CSF, ε4HMZ continued to have significantly greater structural covariance in IC29 ($F_{3,121} = 16.82$; $P = 0.001$) (Fig. 2C), and, most importantly, this was confirmed when we restricted the analysis to those with negative CSF $A\beta_{42}$ ($F_{3,71} = 7.18$; $P = 0.009$) (Fig. 2D), indicating that these effects were independent on amyloid. Conversely, the modulatory role of *APOE*-ε4 on the structural coupling between IC10 and IC15 observed in the entire sample was not confirmed when inspected in amyloid negative subjects ($F_{5,71} = 0.15$;

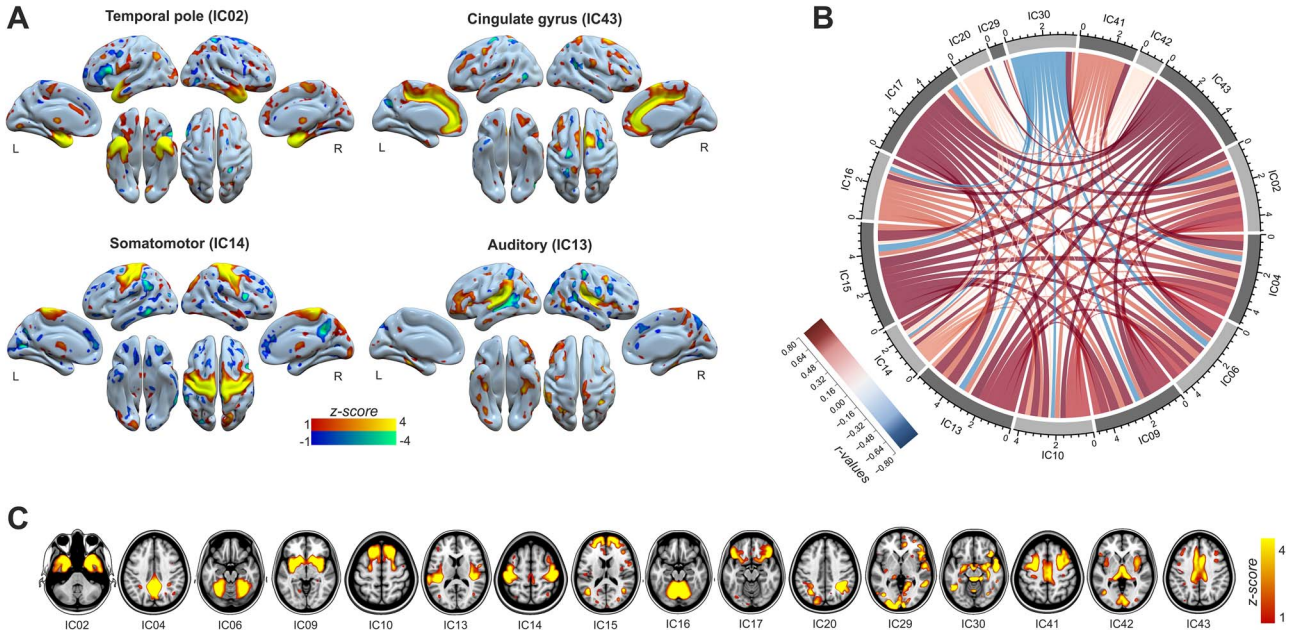

Figure 1. Structural GMn. (*A*) Surface rendering of four exemplary GMn identified in our sample with structural ICA. In each network, warm colors (red–yellow) indicate areas that are significantly related among each other in terms of GM volume. Cold colors (green–blue) denote the anticorrelation network, that is, brain regions that display a negative correlation with the areas in the positive correlation network. (*B*) Chord diagram illustrating the correlation matrix among all the 16 structural networks. Each sector along the circle, measured by arbitrary bin units in canvas coordinates, represents one structural network, with the length denoting the total amount of connections of each network. The thickness of inner ribbons indicates the strength of the correlation, while the sign is encoded by the color. (*C*) Volume rendering of the 16 structural components projected over axial slices, at their respective global maximum standardized coordinate.

Table 2 Brain regions included in IC29

Brain region	Peak intensity	Laterality	*k*	Peak MNI coordinates		
				x	y	z
Cerebellar Crus 2	8.48	L	8022	-42	−51	−34
Precuneus	6.13	R	12 126	18	−60	19
Angular gyrus	4.93	R	3132	43	−42	39
Superior parietal	3.87	R	680	21	−48	60
Temporal pole	3.41	R	3921	46	9	−36
Superior frontal	3.31	L	1314	−13	0	66
Middle frontal	3.23	R	409	30	42	21
Superior parietal	3.01	L	211	−19	−70	55
Middle frontal	2.96	L	141	−24	4.5	49
Middle temporal	2.78	L	757	−42	−61	13
Inferior temporal	2.73	L	106	−55	−31	−18
Precuneus	2.65	L	220	−9	−60	45
Middle temporal	2.48	R	296	54	−51	0
Orbitofrontal	2.47	R	351	7.5	40	−4
Inf. front. (Tri)	2.41	R	1033	49	22	4
Middle frontal	2.38	R	267	36	9	43
Inf. front. (Orb)	2.07	L	103	−27	16	−25

Note: *k*: cluster size, indicates the number of contiguous voxels within each cluster. MNI: Montreal Neurological Institute.

$P = 0.71$), suggesting that this effect may be related to the presence of amyloid.

Gray Matter Networks and Their Association with Cognitive Performance

We found significantly negative linear association between all GMn and age, with the exception of IC20, which entangled the bilateral superior parietal cortex. Partial correlations did not reveal significant relationships between any GMn and EM. However, for PS, we observed significantly positive associations in four networks as well as significantly negative associations in two networks (Table 3).

Discussion

We have reported that *APOE*-ε4 risk variant for AD exerts a significant impact on intrinsic GMn in cognitively unimpaired middle-aged individuals.

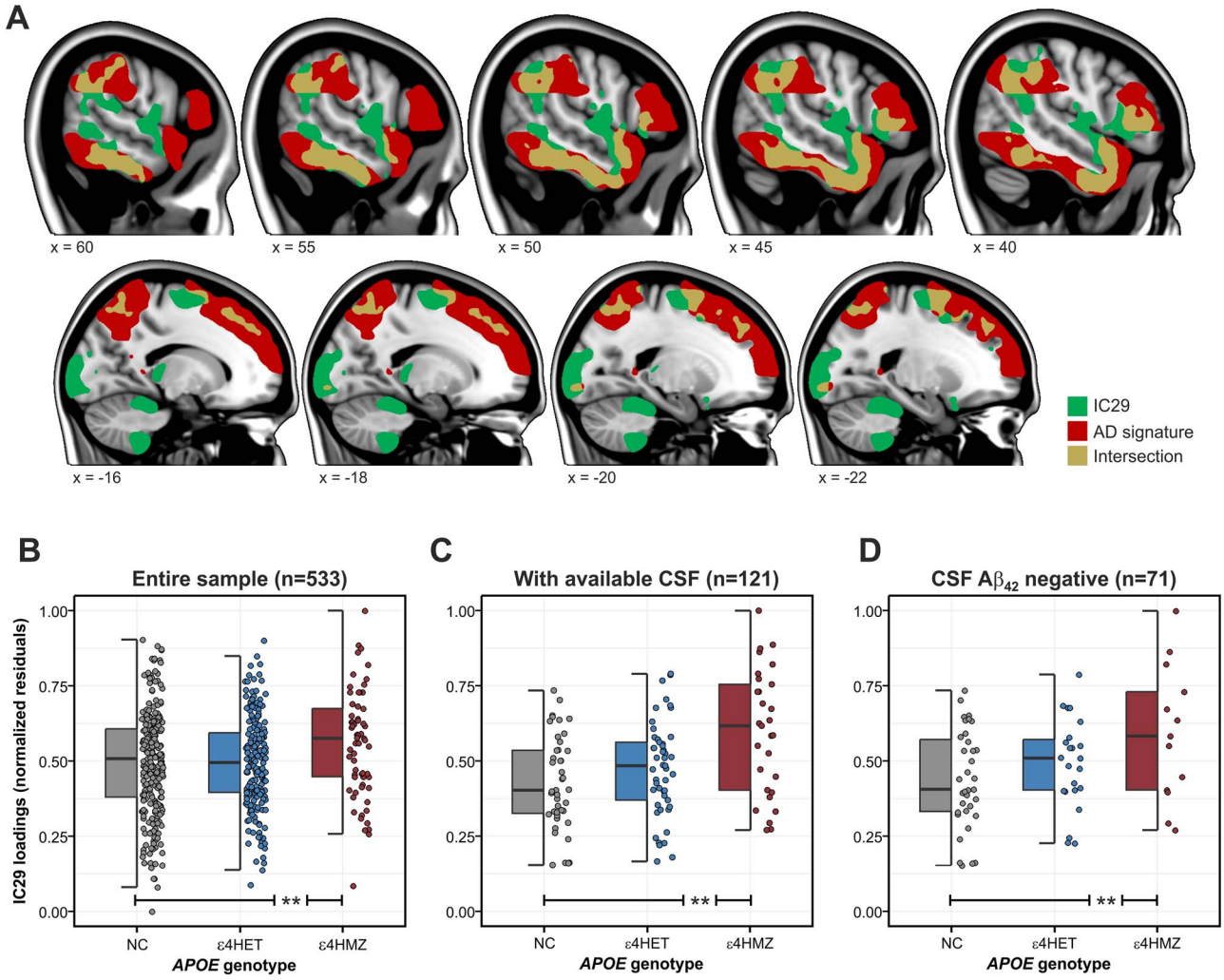

Figure 2. *APOE-ε4* homozygotes showed altered structural brain covariance. (*A*) Volume rendering of IC29 overlaid on the AD-signature composite region of interest, projected over sagittal slides. Brown areas indicate the spatial overlay between the two rendered volumes, which was evident in the inferior parietal, frontal as well as middle and inferior temporal areas and the precuneus. (*B–D*) Boxplot charts showing significantly heightened structural covariance of IC29 in *APOE-ε4* homozygotes compared with both NC and heterozygotes. The width of each box indicate the interquartile range, with the horizontal line showing the median. Data from each individual are shown in a separate vertical column. NC: noncarriers; ε4HET: *APOE-ε4* heterozygotes; and ε4HMZ: *APOE-ε4* homozygotes.

Table 3 Linear correlations between GMn and PS in the entire sample

Component	*r*-value	*P*	P_{FWE}
Positive correlations			
IC02	0.13	0.004	0.02
IC13	0.14	0.001	0.02
IC15	0.15	0.001	0.01
IC16	0.12	0.001	0.01
Negative correlations			
IC29	−0.12	0.006	0.02
IC30	−0.12	0.002	0.02

Our approach of retrieving naturally grouping sources of structural covariance within a sample hosting an unprecedented number of ε4HMZ ($n = 65$) allowed us to unmask a latent structural vulnerability imaging phenotype associated to this risk variant. Within-network analysis revealed that cognitively intact ε4HMZ had increased structural covariance in one network (IC29), which included prominently right lateralized parietal, inferior frontal, as well as inferior and middle temporal regions. In addition, this network entangled the left angular gyrus, precuneus, as well as the left middle and inferior temporal cortex. IC29 exhibited the least degree of covariance with the rest of networks, indicating that its variability was not related to the topological patterns in the rest of the brain. Moreover, it was negatively associated to PS performance across the entire sample. Overall, this suggests that IC29 captures an intrinsic structural organization of the brain that expresses a pathological process. In support of this, we have observed that nearly all the regions included in such a network are part of a previously described composite region of interest, which undergoes focal atrophy early in the course of AD, the so-called "AD-signature" (Bakkour et al., 2009, 2013; Dickerson et al., 2009, 2011). Other research groups detected selective cortical thinning in the same areas of the AD-signature both in AD and MCI patients

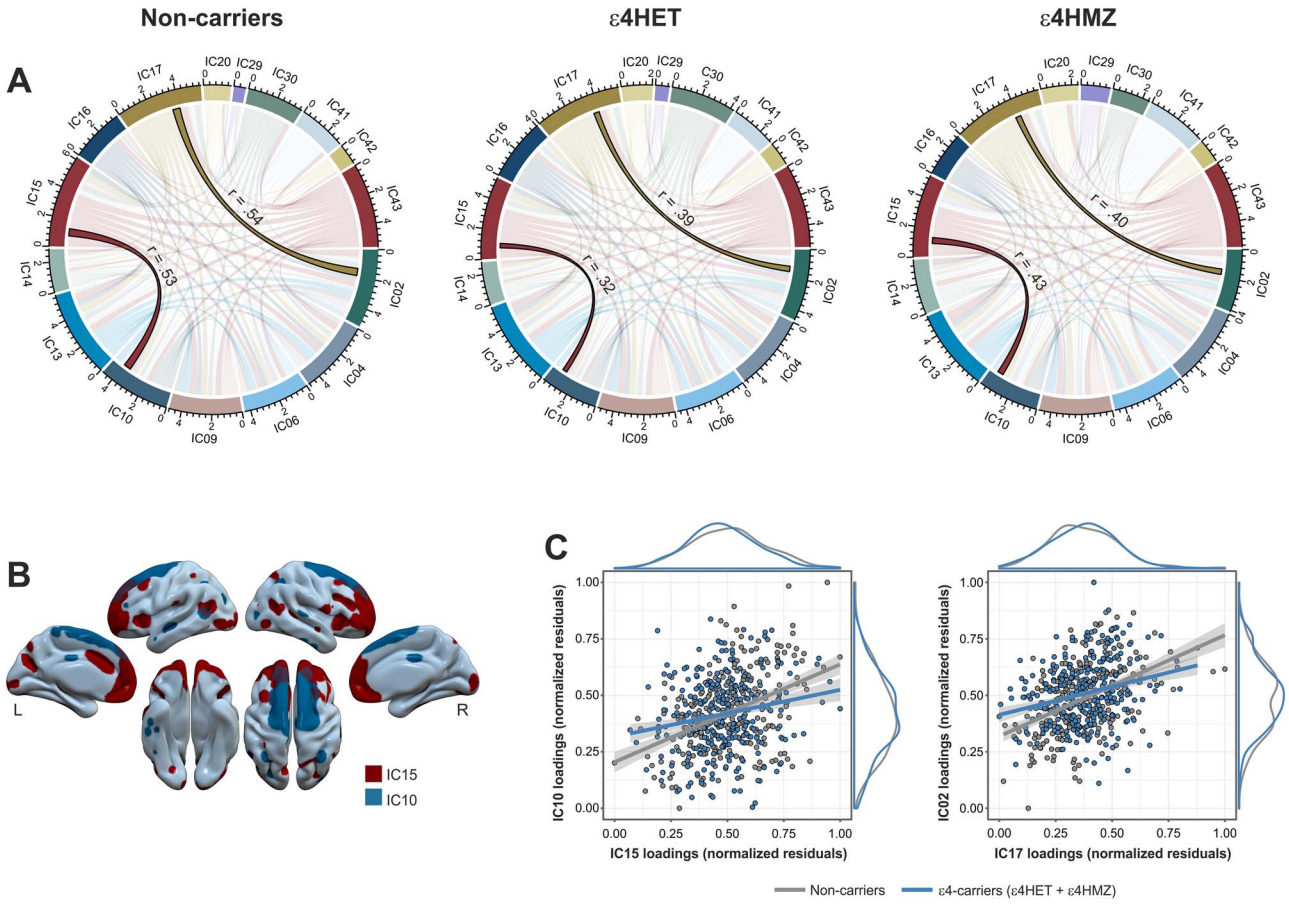

Figure 3. *APOE*-ε4 carriers display reduced connectivity between two pairs of structural networks. (*A*) Chord diagrams computed for each *APOE* subgroups highlighting the two network couplings (IC10/IC15 and IC02/IC17), which were affected by the *APOE*-ε4 genotype. The length of each outer sector is measured by arbitrary bin units in canvas coordinates and encodes the total amount of connections of a given network. The thickness inside each chord diagram encodes the strength of correlation. NC: noncarriers; ε4HET: *APOE*-ε4 heterozygotes; and ε4HMZ: *APOE*-ε4 homozygotes. (*B*) Surface rendering of the binarized IC10 and IC15, where an FDR-surviving significant effect of *APOE*-ε4 was found. (*C*) Group scatterplots with marginal densities reported aside each axes, showing the modulatory effect of *APOE*-ε4 on the linear association between two pairs of component. Shaded areas around the fitted regression lines indicated 90% confidence interval.

(Singh et al., 2006). These brain regions are also typically subject to hypometabolism in preclinical (Besson et al., 2015) and full-blown AD dementia (Alexander et al., 2002; Mosconi, 2013), as well as in cognitively unimpaired *APOE*-ε4 carriers compared with NC (Reiman et al., 2005; Mosconi et al., 2008). It is worth noting that the temporal and parietal areas included in IC29 have been previously described as "cortical hubs," that is, heteromodal regions interconnecting spatially distributed and functionally specialized brain systems, which, possibly because of their higher metabolic consumption rates, are especially vulnerable to the AD neurodegenerative process (Buckner et al., 2009; Sepulcre et al., 2012). Finally, IC29 overlaps with the anterior subdivision of the DMN (Xu et al., 2016; Staffaroni et al., 2018), which is known for being vulnerable in AD (Buckner et al., 2005; Seeley et al., 2009).

Since its definition, the AD-signature has been validated as effective diagnostic and prognostic marker. Some studies demonstrated that AD-signature cortical thinning outperforms hippocampal volume in predicting conversion from MCI to AD (Dickerson et al., 2011; Dickerson and Wolk, 2013). Dickerson and Wolk (2013) reported the superior sensitivity of AD-signature cortical thinning over both amyloid and tau fluid biomarkers in predicting AD dementia onset within 1 year from baseline assessment. One study demonstrated that cortical thinning in these regions was related to suprathreshold CSF tau levels in cognitively unimpaired individuals (Wang et al., 2015). In the same study, the authors reported that AD-signature cortical thinning was negatively related to visuospatial processing (Wang et al., 2015), which is consistent with the negative association we observed between IC29 factor loadings and PS. Notably, even though the AD-signature was initially detected on the basis of cortical thickness data, the same regions were retrieved when comparing AD patients with asymptomatic individuals adopting a voxel-wise method, a technique similar to the one used in the present study (Schwarz et al., 2016). In line with this, exploratory studies employing voxel-based morphometry found that, among MCI patients, only those who later progressed to AD dementia showed, compared with healthy controls, volume reductions in AD-signature areas (Chételat et al., 2005; Bozzali et al., 2006; Whitwell et al., 2008). In our previous study conducted on the same sample as the one of the present report, we did not find volume difference among *APOE*-ε4 subgroups in these regions (Cacciaglia et al., 2018a). Hence, our data suggest that an increased structural covariance within the AD-signature areas in individuals exposed to exceptionally high risk for AD, such as *APOE*-ε4 homozygotes, may predate cortical thinning

as well as hypometabolism in these regions. Moreover, an exaggerated connectivity among these brain areas may facilitate the patterned spreading of AD proteinopathies within this network, which is well-known for being particularly vulnerable to AD pathology (Zhou et al., 2012; Ossenkoppele et al., 2019).

Importantly, we replicated this finding in a subsample of individuals who had no signs of incipient amyloid accumulation as revealed by negative CSF $A\beta_{42}$ biomarker, indicating that it was specifically due to *APOE* genetic variance. This strongly suggests that ε4HMZ harbor a structural brain vulnerability that precedes amyloidosis and supports earlier findings of *APOE*-ε4 related effects on neurodevelopment (Shaw et al., 2007; Wolf et al., 2013; Chang et al., 2016). In line with this, some studies have observed AD-signature cortical thinning in association with CSF tau levels in asymptomatic, amyloid negative, and subjects (Wang et al., 2015). In addition, *APOE*-ε4 has been found to have an impact on temporoparietal FDG uptake in cognitively healthy individuals who were Aβ negative (Jagust et al., 2012), suggesting that its effects on neurodegeneration markers may occur earlier or independently on amyloid.

Nevertheless, the cross-sectional nature of our study prevents us to draw this conclusion and our data foster upcoming studies to assess GMn in longitudinal settings.

It is worth noting that the relatively high prevalence of amyloid positive individuals in the subset with available CSF data ($n = 171$, 29% with positive CSF $A\beta_{42}$) is not surprising, given that our sample was enriched for the genetic risk of AD, according to the selection criteria employed in the ALFA study (Molinuevo et al., 2016).

We should note that IC29 was predominantly right-lateralized, with relatively few and regions appearing in the left hemisphere. Our data, however, indicate that the magnitude of this component was associated with the presence of ε4HMZ. The relative poor representation of this subgroup in the entire sample (65 out of 533 individuals) may have caused some loss of signal, resulting in a spatial inhomogeneity. It is possible that a more balanced sample with an equal number of NC and heterozygotes as homozygotes would lead to a bilateral distribution. On the other hand, as noted above, the spatial topology of IC29 overlaps with the anterior subdivision of DMN (Xu et al., 2016; Staffaroni et al., 2018). This is in general not surprising given that networks of structural and functional covariance share the same topology (Alexander-Bloch et al., 2018, Smith et al., 2019). In cognitively healthy individuals, the DMN was found to be mostly left-lateralized with aging shifting this lateralization to the right side (Agcaoglu et al., 2015). Interestingly, age-related right-lateralization of the anterior DMN predicts poorer cognitive outcomes (Banks et al., 2018), supporting our data on the negative relationship between IC29 and PS. Thus, the predominantly right-lateralized topology of IC29 may represent an additional indicator of an aging-related pathological process, encapsulated by this component.

When performing the between-networks analysis, we found that compared with NC, *APOE*-ε4 carriers had significantly decreased structural covariance between IC10 and IC15. The former component included medial and lateral aspects of the superior frontal cortex bilaterally, with the inclusion of the middle cingulate gyrus, while the latter entangled the frontal poles as well as the anterior cingulate cortex and bilateral middle temporal gyrus (Fig. 3B). All of these regions constitute preferential target of early Aβ deposition (Klunk et al., 2004; Myers et al., 2014; Grothe et al., 2017). Notably, unlike for the previous finding on the increased covariance within IC29, we could not replicate this result when restricting the analysis to amyloid-negative subjects. This might be due to the reduced statistical power given the lower sample size or be associated to a putative role of amyloid. In support of the latter, earlier studies have shown that cortical Aβ deposition impairs synaptic transmission and consequently reduces the local functional connectivity between the affected circuits (Lacor et al., 2007; Palop and Mucke, 2010). Thus, it is possible that incipient cortical Aβ deposition associated with the presence of *APOE*-ε4 allele impairs the structural covariance between these two networks in asymptomatic individuals. This result may represent an AD intermediate phenotype in a way that it reflects a network disconnection, in line with the "disconnection hypothesis" of AD (Delbeuck et al., 2003; Reid and Evans, 2013; Sepulcre et al., 2013), possibly due to impairment in synaptic communication. Finally, it is worth noting that the reduced covariance between IC10 and IC15 was significant under a genotypic dominance assumption, indicating that the effect was common to the heterozygote and homozygote groups, compared with NC. In other words, this neuroimaging phenotype was detectable already in a subgroup, the ε4HET, which is moderately exposed to the genetic risk of AD, compared with the ε4HMZ (Liu et al., 2013). This suggests that the two imaging findings reported here may reflect distinct levels of the genetic risk for AD, which appear to be hierarchically organized.

Taken together, our results indicate that *APOE*-ε4 shapes the cerebral organization in middle-age asymptomatic individuals, even in individuals with no amyloid pathology, in a way that recapitulates focal morphometric alterations observed in MCI and AD patients. This provides new insights for the structural vulnerability associated to this highly penetrant risk variant. Our study promotes the use of structural covariance networks as a valuable AD intermediate phenotype, which may be subject to change earlier than cortical thinning or volume loss. Future studies shall track GMn in longitudinal designs along with more extensive biomarkers screening to further address potential interaction between AD-related pathology and *APOE* genetic variance.

Supplementary Material

Supplementary material is available at *Cerebral Cortex* online.

Funding

"la Caixa" Foundation (ID 100010434), under agreement LCF/PR/GN17/50300004, and the Alzheimer's Association and an international anonymous charity foundation through the TriBEKa Imaging Platform project (TriBEKa-17-519007). Additional support has been received from the Universities and Research Secretariat, Ministry of Business and Knowledge of the Catalan Government under the grant no. 2017-SGR-892. J.D.G. is supported by the Spanish Ministry of Economy, and Competitiveness (RYC-2013-13054).

Notes

This publication is part of the ALFA study (ALzheimer and FAmilies). The authors would like to express their most sincere gratitude to the ALFA project participants, without whom this research would have not been possible. Authors would like to thank Roche Diagnostics International Ltd for kindly providing the kits for the CSF analysis of ALFA participants. Collaborators

of the ALFA study are: Alba Cañas, Carme Deulofeu, Ruth Dominguez, Karine Fauria, Marta Félez-Sánchez, José M. González de Echevarri, Oriol Grau-Rivera, Laura Hernandez, Gema Huesa, Jordi Huguet, Paula Marne, Tania Menchón, Marta Milà-Alomà, Carolina Minguillon, Grégory Operto, Maria Pascual, Albina Polo, Sandra Pradas, Aleix Sala-Vila, Anna Soteras, Marc Suárez-Calvet, Laia Tenas, Marc Vilanova, and Natalia Vilor-Tejedor. ELECSYS, COBAS, and COBAS E are registered trademarks of Roche.

J.L.M. has served/serves as a consultant or at advisory boards for the following for-profit companies, or has given lectures in symposia sponsored by the following for-profit companies: Roche Diagnostics, Genentech, Novartis, Lundbeck, Oryzon, Biogen, Lilly, Janssen, Green Valley, MSD, Eisai, Alector, BioCross, GE Healthcare, and ProMIS Neurosciences. K.B. has served as a consultant or at advisory boards for Abcam, Axon, Biogen, Lilly, MagQu, Novartis, and Roche Diagnostics, and is a cofounder of Brain Biomarker Solutions in Gothenburg AB, a GU Venture-based platform company at the University of Gothenburg, all unrelated to the work presented in this paper. H.Z. has served at scientific advisory boards for Samumed, CogRx, Wave, and Roche Diagnostics, has given lectures in symposia sponsored by Biogen and Alzecure, and is a cofounder of Brain Biomarker Solutions in Gothenburg AB, a GU Ventures-based platform company at the University of Gothenburg. The rest of authors have nothing to disclose. *Conflict of Interest:* None declared.

References

Agcaoglu O, Miller R, Mayer AR, Hugdahl K, Calhoun VD. 2015. Lateralization of resting state networks and relationship to age and gender. *NeuroImage*. 104:310–325.

Alexander GE, Bergfield KL, Chen K, Reiman EM, Hanson KD, Lin L, Bandy D, Caselli RJ, Moeller JR. 2012. Gray matter network associated with risk for Alzheimer's disease in young to middle-aged adults. *Neurobiol Aging*. 33:2723–2732.

Alexander GE, Chen K, Pietrini P, Rapoport SI, Reiman EM. 2002. Longitudinal PET evaluation of cerebral metabolic decline in dementia: a potential outcome measure in Alzheimer's disease treatment studies. *Am J Psychiatry*. 159: 738–745.

Alexander-Bloch A, Giedd JN, Bullmore E. 2013. Imaging structural co-variance between human brain regions. *Nat Rev Neurosci*. 14:322–336.

Alexander-Bloch AF, Shou H, Liu S, Satterthwaite TD, Glahn DC, Shinohara RT, Vandekar SN, Raznahan A. 2018. On testing for spatial correspondence between maps of human brain structure and function. *NeuroImage*. 178:540–551.

Ashburner J. 2007. A fast diffeomorphic image registration algorithm. *NeuroImage*. 38:95–113.

Bakkour A, Morris JC, Dickerson BC. 2009. The cortical signature of prodromal AD: regional thinning predicts mild AD dementia. *Neurology*. 72:1048–1055.

Bakkour A, Morris JC, Wolk DA, Dickerson BC. 2013. The effects of aging and Alzheimer's disease on cerebral cortical anatomy: specificity and differential relationships with cognition. *NeuroImage*. 76:332–344.

Banks SJ, Zhuang X, Bayram E, Bird C, Cordes D, Caldwell JZK, Cummings JL, Alzheimer's Disease Neuroimaging I. 2018. Default mode network lateralization and memory in healthy aging and Alzheimer's disease. *J Alzheimer's Dis: JAD*. 66:1223–1234.

Bell AJ, Sejnowski TJ. 1995. An information-maximization approach to blind separation and blind deconvolution. *Neural Comput*. 7:1129–1159.

Benjamini Y, Hochberg Y. 1995. Controlling the false discovery rate: a practical and powerful approach to multiple testing. *J R Stat Soc Ser B Methodol*. 57:289–300.

Besson FL, La Joie R, Doeuvre L, Gaubert M, Mezenge F, Egret S, Landeau B, Barre L, Abbas A, Ibazizene M *et al*. 2015. Cognitive and brain profiles associated with current neuroimaging biomarkers of preclinical Alzheimer's disease. *J Neurosci Off J Soc Neurosci*. 35:10402–10411.

Bittner T, Zetterberg H, Teunissen CE, Ostlund RE Jr, Militello M, Andreasson U, Hubeek I, Gibson D, Chu DC, Eichenlaub U *et al*. 2016. Technical performance of a novel, fully automated electrochemiluminescence immunoassay for the quantitation of beta-amyloid (1–42) in human cerebrospinal fluid. *Alzheimer's Dement: J Alzheimer's Assoc*. 12:517–526.

Bozzali M, Filippi M, Magnani G, Cercignani M, Franceschi M, Schiatti E, Castiglioni S, Mossini R, Falautano M, Scotti G *et al*. 2006. The contribution of voxel-based morphometry in staging patients with mild cognitive impairment. *Neurology*. 67:453–460.

Braskie MN, Thompson PM. 2013. Understanding cognitive deficits in Alzheimer's disease based on neuroimaging findings. *Trends Cogn Sci*. 17:510–516.

Buckner RL, Sepulcre J, Talukdar T, Krienen FM, Liu H, Hedden T, Andrews-Hanna JR, Sperling RA, Johnson KA. 2009. Cortical hubs revealed by intrinsic functional connectivity: mapping, assessment of stability, and relation to Alzheimer's disease. *J Neurosci Off J Soc Neurosci*. 29:1860–1873.

Buckner RL, Snyder AZ, Shannon BJ, LaRossa G, Sachs R, Fotenos AF, Sheline YI, Klunk WE, Mathis CA, Morris JC *et al*. 2005. Molecular, structural, and functional characterization of Alzheimer's disease: evidence for a relationship between default activity, amyloid, and memory. *J Neurosci Off J Soc Neurosci*. 25:7709–7717.

Buschke H. 2014. Rationale of the memory binding test. In: Nilsson L, Ohta N, editors. *Dementia and memory*. Hove, East Sussex: Psychology Press, pp. 55–71.

Cacciaglia R, Molinuevo JL, Falcon C, Brugulat-Serrat A, Sanchez-Benavides G, Gramunt N, Esteller M, Moran S, Minguillon C, Fauria K *et al*. 2018a. Effects of APOE-epsilon4 allele load on brain morphology in a cohort of middle-aged healthy individuals with enriched genetic risk for Alzheimer's disease. *Alzheimer's Dement: J Alzheimer's Assoc*. 14:902–912.

Cacciaglia R, Molinuevo JL, Falcon C, Sanchez-Benavides G, Gramunt N, Brugulat-Serrat A, Esteller M, Moran S, Fauria K, Gispert JD *et al*. 2019. APOE-epsilon4 risk variant for Alzheimer's disease modifies the association between cognitive performance and cerebral morphology in healthy middle-aged individuals. *NeuroImage Clin*. 23:101818.

Cacciaglia R, Molinuevo JL, Sanchez-Benavides G, Falcon C, Gramunt N, Brugulat-Serrat A, Grau O, Gispert JD, Study A. 2018b. Episodic memory and executive functions in cognitively healthy individuals display distinct neuroanatomical correlates which are differentially modulated by aging. *Hum Brain Mapp*. 39:4565–4579.

Chang L, Douet V, Bloss C, Lee K, Pritchett A, Jernigan TL, Akshoomoff N, Murray SS, Frazier J, Kennedy DN *et al*. 2016. Gray matter maturation and cognition in children with different APOE epsilon genotypes. *Neurology*. 87:585–594.

Chételat G, Landeau B, Eustache F, Mezenge F, Viader F, de la Sayette V, Desgranges B, Baron JC. 2005. Using voxel-based

morphometry to map the structural changes associated with rapid conversion in MCI: a longitudinal MRI study. *NeuroImage*. 27:934–946.

Clarke GM, Anderson CA, Pettersson FH, Cardon LR, Morris AP, Zondervan KT. 2011. Basic statistical analysis in genetic case-control studies. *Nat Protoc*. 6:121–133.

Corder EH, Saunders AM, Strittmatter WJ, Schmechel DE, Gaskell PC, Small GW, Roses AD, Haines JL, Pericak-Vance MA. 1993. Gene dose of apolipoprotein E type 4 allele and the risk of Alzheimer's disease in late onset families. *Science*. 261:921–923.

Delbeuck X, Van der Linden M, Collette F. 2003. Alzheimer's disease as a disconnection syndrome? *Neuropsychol Rev*. 13:79–92.

Dickerson BC, Bakkour A, Salat DH, Feczko E, Pacheco J, Greve DN, Grodstein F, Wright CI, Blacker D, Rosas HD *et al*. 2009. The cortical signature of Alzheimer's disease: regionally specific cortical thinning relates to symptom severity in very mild to mild AD dementia and is detectable in asymptomatic amyloid-positive individuals. *Cereb Cortex*. 19:497–510.

Dickerson BC, Stoub TR, Shah RC, Sperling RA, Killiany RJ, Albert MS, Hyman BT, Blacker D, Detoledo-Morrell L. 2011. Alzheimer-signature MRI biomarker predicts AD dementia in cognitively normal adults. *Neurology*. 76:1395–1402.

Dickerson BC, Wolk DA, Alzheimer's Disease Neuroimaging I. 2013. Biomarker-based prediction of progression in MCI: comparison of AD signature and hippocampal volume with spinal fluid amyloid-beta and tau. *Front Aging Neurosci*. 5:55.

Donohue MC, Sperling RA, Salmon DP, Rentz DM, Raman R, Thomas RG, Weiner M, Aisen PS, Australian Imaging B, Lifestyle Flagship Study of A, Alzheimer's Disease Neuroimaging I, Alzheimer's Disease Cooperative S. 2014. The preclinical Alzheimer cognitive composite: measuring amyloid-related decline. *JAMA Neurol*. 71:961–970.

Eckert MA, Keren NI, Roberts DR, Calhoun VD, Harris KC. 2010. Age-related changes in processing speed: unique contributions of cerebellar and prefrontal cortex. *Front Hum Neurosci*. 4:10.

Escott-Price V, Sims R, Bannister C, Harold D, Vronskaya M, Majounie E, Badarinarayan N, Gerad/Perades, consortia I, Morgan K, Passmore P *et al*. 2015. Common polygenic variation enhances risk prediction for Alzheimer's disease. *Brain J Neurol*. 138:3673–3684.

Evans AC. 2013. Networks of anatomical covariance. *NeuroImage*. 80:489–504.

Farrer LA, Cupples LA, Haines JL, Hyman B, Kukull WA, Mayeux R, Myers RH, Pericak-Vance MA, Risch N, van Duijn CM. 1997. Effects of age, sex, and ethnicity on the association between apolipoprotein E genotype and Alzheimer disease. A meta-analysis. APOE and Alzheimer disease meta analysis consortium. *JAMA*. 278:1349–1356.

Fouquet M, Besson FL, Gonneaud J, La Joie R, Chetelat G. 2014. Imaging brain effects of APOE4 in cognitively normal individuals across the lifespan. *Neuropsychol Rev*. 24:290–299.

Frisoni GB, Boccardi M, Barkhof F, Blennow K, Cappa S, Chiotis K, Demonet JF, Garibotto V, Giannakopoulos P, Gietl A *et al*. 2017. Strategic roadmap for an early diagnosis of Alzheimer's disease based on biomarkers. *Lancet Neurol*. 16:661–676.

Good CD, Johnsrude IS, Ashburner J, Henson RN, Friston KJ, Frackowiak RS. 2001. A voxel-based morphometric study of ageing in 465 normal adult human brains. *NeuroImage*. 14:21–36.

Gramunt N, Sanchez-Benavides G, Buschke H, Dieguez-Vide F, Pena-Casanova J, Masramon X, Fauria K, Gispert JD, Molinuevo JL. 2016. The memory binding test: development of two alternate forms into Spanish and Catalan. *J Alzheimer's Dis: JAD*. 52:283–293.

Grothe MJ, Barthel H, Sepulcre J, Dyrba M, Sabri O, Teipel SJ, Alzheimer's Disease Neuroimaging I. 2017. In vivo staging of regional amyloid deposition. *Neurology*. 89:2031–2038.

Guo X, Chen K, Zhang Y, Wang Y, Yao L. 2014. Regional covariance patterns of gray matter alterations in Alzheimer's disease and its replicability evaluation. *J Magn Reson Imaging: JMRI*. 39:143–149.

Himberg J, Hyvarinen A, Esposito F. 2004. Validating the independent components of neuroimaging time series via clustering and visualization. *NeuroImage*. 22:1214–1222.

Honea RA, Vidoni E, Harsha A, Burns JM. 2009. Impact of APOE on the healthy aging brain: a voxel-based MRI and DTI study. *J Alzheimer's Dis: JAD*. 18:553–564.

Jagust WJ, Landau SM, Alzheimer's Disease Neuroimaging I. 2012. Apolipoprotein E, not fibrillar beta-amyloid, reduces cerebral glucose metabolism in normal aging. *J Neurosci Off J Soc Neurosci*. 32:18227–18233.

Jansen WJ, Ossenkoppele R, Knol DL, Tijms BM, Scheltens P, Verhey FR, Visser PJ, Amyloid Biomarker Study G, Aalten P, Aarsland D *et al*. 2015. Prevalence of cerebral amyloid pathology in persons without dementia: a meta-analysis. *JAMA*. 313:1924–1938.

Kasparek T, Marecek R, Schwarz D, Prikryl R, Vanicek J, Mikl M, Ceskova E. 2010. Source-based morphometry of gray matter volume in men with first-episode schizophrenia. *Hum Brain Mapp*. 31:300–310.

Klunk WE, Engler H, Nordberg A, Wang Y, Blomqvist G, Holt DP, Bergstrom M, Savitcheva I, Huang GF, Estrada S *et al*. 2004. Imaging brain amyloid in Alzheimer's disease with Pittsburgh compound-B. *Ann Neurol*. 55:306–319.

Lacor PN, Buniel MC, Furlow PW, Clemente AS, Velasco PT, Wood M, Viola KL, Klein WL. 2007. Abeta oligomer-induced aberrations in synapse composition, shape, and density provide a molecular basis for loss of connectivity in Alzheimer's disease. *J Neurosci Off J Soc Neurosci*. 27:796–807.

Li YO, Adali T, Calhoun VD. 2007. Estimating the number of independent components for functional magnetic resonance imaging data. *Hum Brain Mapp*. 28:1251–1266.

Liu CC, Liu CC, Kanekiyo T, Xu H, Bu G. 2013. Apolipoprotein E and Alzheimer disease: risk, mechanisms and therapy. *Nat Rev Neurol*. 9:106–118.

Molinuevo JL, Gramunt N, Gispert JD, Fauria K, Esteller M, Minguillon C, Sanchez-Benavides G, Huesa G, Moran S, Dal-Re R *et al*. 2016. The ALFA project: a research platform to identify early pathophysiological features of Alzheimer's disease. *Alzheimers Dement (N Y)*. 2:82–92.

Mosconi L. 2013. Glucose metabolism in normal aging and Alzheimer's disease: methodological and physiological considerations for PET studies. *Clin Transl Imag*. 1:217–233.

Mosconi L, De Santi S, Brys M, Tsui WH, Pirraglia E, Glodzik-Sobanska L, Rich KE, Switalski R, Mehta PD, Pratico D *et al*. 2008. Hypometabolism and altered cerebrospinal fluid markers in normal apolipoprotein E E4 carriers with subjective memory complaints. *Biol Psychiatry*. 63:609–618.

Myers N, Pasquini L, Gottler J, Grimmer T, Koch K, Ortner M, Neitzel J, Muhlau M, Forster S, Kurz A *et al*. 2014. Within-patient correspondence of amyloid-beta and intrinsic

network connectivity in Alzheimer's disease. *Brain J Neurol*. 137:2052–2064.

Ossenkoppele R, Iaccarino L, Schonhaut DR, Brown JA, La Joie R, O'Neil JP, Janabi M, Baker SL, Kramer JH, Gorno-Tempini ML *et al*. 2019. Tau covariance patterns in Alzheimer's disease patients match intrinsic connectivity networks in the healthy brain. *NeuroImage Clin*. 23:101848.

Palop JJ, Mucke L. 2010. Amyloid-beta-induced neuronal dysfunction in Alzheimer's disease: from synapses toward neural networks. *Nat Neurosci*. 13:812–818.

Reid AT, Evans AC. 2013. Structural networks in Alzheimer's disease. *Eur Neuropsychopharmacol: J Eur Coll Neuropsychopharmacol*. 23:63–77.

Reiman EM, Chen K, Alexander GE, Caselli RJ, Bandy D, Osborne D, Saunders AM, Hardy J. 2005. Correlations between apolipoprotein E epsilon4 gene dose and brain-imaging measurements of regional hypometabolism. *Proc Natl Acad Sci U S A*. 102:8299–8302.

Reiman EM, Chen K, Liu X, Bandy D, Yu M, Lee W, Ayutyanont N, Keppler J, Reeder SA, Langbaum JB *et al*. 2009. Fibrillar amyloid-beta burden in cognitively normal people at 3 levels of genetic risk for Alzheimer's disease. *Proc Natl Acad Sci U S A*. 106:6820–6825.

Schindler SE, Gray JD, Gordon BA, Xiong C, Batrla-Utermann R, Quan M, Wahl S, Benzinger TLS, Holtzman DM, Morris JC *et al*. 2018. Cerebrospinal fluid biomarkers measured by Elecsys assays compared to amyloid imaging. *Alzheimer's Dement: J Alzheimer's Assoc*. 14:1460–1469.

Schwarz CG, Gunter JL, Wiste HJ, Przybelski SA, Weigand SD, Ward CP, Senjem ML, Vemuri P, Murray ME, Dickson DW *et al*. 2016. A large-scale comparison of cortical thickness and volume methods for measuring Alzheimer's disease severity. *NeuroImage Clin*. 11:802–812.

Seeley WW, Crawford RK, Zhou J, Miller BL, Greicius MD. 2009. Neurodegenerative diseases target large-scale human brain networks. *Neuron*. 62:42–52.

Sepulcre J, Sabuncu MR, Becker A, Sperling R, Johnson KA. 2013. In vivo characterization of the early states of the amyloid-beta network. *Brain J Neurol*. 136:2239–2252.

Sepulcre J, Sabuncu MR, Yeo TB, Liu H, Johnson KA. 2012. Stepwise connectivity of the modal cortex reveals the multimodal organization of the human brain. *J Neurosci Off J Soc Neurosci*. 32:10649–10661.

Shaw P, Lerch JP, Pruessner JC, Taylor KN, Rose AB, Greenstein D, Clasen L, Evans A, Rapoport JL, Giedd JN. 2007. Cortical morphology in children and adolescents with different apolipoprotein E gene polymorphisms: an observational study. *Lancet Neurol*. 6:494–500.

Singh V, Chertkow H, Lerch JP, Evans AC, Dorr AE, Kabani NJ. 2006. Spatial patterns of cortical thinning in mild cognitive impairment and Alzheimer's disease. *Brain J Neurol*. 129:2885–2893.

Smith S, Duff E, Groves A, Nichols TE, Jbabdi S, Westlye LT, Tamnes CK, Engvig A, Walhovd KB, Fjell AM *et al*. 2019. Structural variability in the human brain reflects fine-grained functional architecture at the population level. *J Neurosci Off J Soc Neurosci*. 39:6136–6149.

Sperling RA, Aisen PS, Beckett LA, Bennett DA, Craft S, Fagan AM, Iwatsubo T, Jack CR Jr, Kaye J, Montine TJ *et al*. 2011. Toward defining the preclinical stages of Alzheimer's disease: recommendations from the National Institute on Aging-Alzheimer's Association workgroups on diagnostic guidelines for Alzheimer's disease. *Alzheimer's Dement: J Alzheimer's Assoc*. 7:280–292.

Spreng RN, Turner GR. 2013. Structural covariance of the default network in healthy and pathological aging. *J Neurosci Off J Soc Neurosci*. 33:15226–15234.

Staffaroni AM, Brown JA, Casaletto KB, Elahi FM, Deng J, Neuhaus J, Cobigo Y, Mumford PS, Walters S, Saloner R *et al*. 2018. The longitudinal trajectory of default mode network connectivity in healthy older adults varies as a function of age and is associated with changes in episodic memory and processing speed. *J Neurosci Off J Soc Neurosci*. 38:2809–2817.

Steenwijk MD, Geurts JJ, Daams M, Tijms BM, Wink AM, Balk LJ, Tewarie PK, Uitdehaag BM, Barkhof F, Vrenken H *et al*. 2016. Cortical atrophy patterns in multiple sclerosis are non-random and clinically relevant. *Brain J Neurol*. 139:115–126.

Tan CH, Hyman BT, Tan JJX, Hess CP, Dillon WP, Schellenberg GD, Besser LM, Kukull WA, Kauppi K, McEvoy LK *et al*. 2017. Polygenic hazard scores in preclinical Alzheimer disease. *Ann Neurol*. 82:484–488.

Ten Kate M, Sanz-Arigita EJ, Tijms BM, Wink AM, Clerigue M, Garcia-Sebastian M, Izagirre A, Ecay-Torres M, Estanga A, Villanua J *et al*. 2016. Impact of APOE-varepsilon4 and family history of dementia on gray matter atrophy in cognitively healthy middle-aged adults. *Neurobiol Aging*. 38:14–20.

Wang L, Benzinger TL, Hassenstab J, Blazey T, Owen C, Liu J, Fagan AM, Morris JC, Ances BM. 2015. Spatially distinct atrophy is linked to beta-amyloid and tau in preclinical Alzheimer disease. *Neurology*. 84:1254–1260.

Wechsler D. 2012. *WAIS-IV, Escala de inteligencia de Wechsler para adultos-IV*. Madrid: Pearson.

Whitwell JL, Shiung MM, Przybelski SA, Weigand SD, Knopman DS, Boeve BF, Petersen RC, Jack CR Jr. 2008. MRI patterns of atrophy associated with progression to AD in amnestic mild cognitive impairment. *Neurology*. 70:512–520.

Wolf AB, Valla J, Bu G, Kim J, LaDu MJ, Reiman EM, Caselli RJ. 2013. Apolipoprotein E as a beta-amyloid-independent factor in Alzheimer's disease. *Alzheimers Res Ther*. 5:38.

Xu L, Groth KM, Pearlson G, Schretlen DJ, Calhoun VD. 2009. Source-based morphometry: the use of independent component analysis to identify gray matter differences with application to schizophrenia. *Hum Brain Mapp*. 30: 711–724.

Xu X, Yuan H, Lei X. 2016. Activation and connectivity within the default mode network contribute independently to future-oriented thought. *Sci Rep*. 6:21001.

Yoon YB, Shin WG, Lee TY, Hur JW, Cho KIK, Sohn WS, Kim SG, Lee KH, Kwon JS. 2017. Brain structural networks associated with intelligence and visuomotor ability. *Sci Rep*. 7:2177.

Zhou J, Gennatas ED, Kramer JH, Miller BL, Seeley WW. 2012. Predicting regional neurodegeneration from the healthy brain functional connectome. *Neuron*. 73:1216–1227.